Agile Space Object Custody for Electro-Optical Sensors

Johnathan Tucker
Daniel Aguilar-Marsillach

Anna Montgomery

Marcus J. Holzinger
University of Colorado Boulder

ABSTRACT

Using optimal control formulations of reachability analysis a bounding sphere of possible locations of a space object, after some time horizon, can be created. Projecting this sphere onto the focal plane of a telescope allows for the determination of a degree of custody. Here custody represents the knowledge that, at any time, the observing sensor can look at and acquire the space object in question. In this paper, an efficient algorithm that computes the time horizon when the space object will no longer be within a sensor field of view is presented, providing rigorous estimates as to when sensor custody of the SO may be lost. As a consequence, this work improves current telescope tasking and SO tracking methodologies. Given the increase in space objects and limited sensing resources, computationally efficient algorithms that allow for the determination of both custody and the time until custody is potentially lost are highly desirable. This type of analysis can inform sensor tasking strategies for terrestrial, space-based, and cislunar sensor platforms.

1. INTRODUCTION

The United States Space Force defines space domain awareness (SDA) as "the effective identification, characterization, and understanding of any factor associated with the space domain" [1]. It should be recognized that, with the ever increasing population of cislunar space objects, SDA is a big data problem. Here each data point has unstable dynamics that make them difficult to track and therefore also difficult to maintain custody of or re-acquire. This problem demands a combination of solutions such as ground and space based observers as well as efficient custody determination and telescope tasking algorithms [2]. This paper aims to provide the ability to determine custody and task telescopes efficiently for both space and ground based observers. More specifically, the work fundamentally aims to make ground and space-based observers more robust against SO maneuvers. The absence of prior work, particularly for space objects (SOs) in the cislunar domain, motivates the need and challenge of this work.

Past work has shown that by applying optimal control methods and reachability analysis, one can create a sphere that over-approximates the set of reachable positions of an SO after a specified time horizon. This is generally achieved by computing the largest possible position reachable set, which requires solving an optimal control problem for every state on the boundary of an initial set. The largest possible reachable set can be obtained by considering minimum-time optimal controllers with constrained actuation or thrust [3]. The literature has also shown that there are many approaches to computing position reachable sets such as Hamilton-Jacobi-Bellman (HJB) Partial Differential Equation (PDE) solutions for a set, non-optimal control formulations, ellipsoidal and polytopic over and under-approximations, or sampling-based methods using optimal control [3][4][5][6]. The latter provides a tractable solution to approximate the reach set in a computationally efficient manner. Finally, previous work has shown that the position reachable set can be projected onto the focal plane of a telescope for custody determination[7].

This paper conceptually extends the above work by using sampling-based optimal control methods to calculate the position reachable space, which is then projected onto the focal plane or measurement space of a telescope at varying time horizons. Ultimately, this allows operators to compute how long the telescope does not have to actively observe before custody is lost, i.e., the object cannot maneuver out of the sensor field of view in the computed time horizon. Furthermore, this paper extends the above capabilities of reachability analysis by implementing it on both ground and space based observers for custody determination. This will be accomplished through simulations based on real-world

scenarios to ultimately show these methods can be used for efficient telescope tasking and custody determination. The first set of simulations are relevant to an observer maintaining custody of a space object near each of the five Lagrange points. The next simulation simulation scenario has an observer maintaining custody of a space object in a highly elliptical near-rectilinear halo orbit (NRHO), such as the Lunar Gateway. In summary, this paper extends past reachable set determination work presented in Section II by presenting an algorithm in Section III that is used to determine the custody time horizon of a space object. Furthermore, Section IV provides two sets of simulations with a variety of real-world applications and details the computational efficiency of the presented method for custody determination.

2. THEORY

2.1 Hamilton Jacobi Bellman PDE

Prior to the discussion of sampling methods for reachable set computations, the general definition of the optimal control problem (OCP) is introduced. This general form is known as the Bolza OCP given by

$$\sup_{u\in U} \int_{t_0}^{t_f} \mathscr{L}(x(\tau),u(\tau),\tau)d\tau + V(x_f,t_f) \tag{1a}$$

$$\dot{x} = f(x,u,t), \tag{1b}$$

$$h(x,t) \leq 0, \tag{1c}$$

$$g(x_0,t_0,x_f,t_f) = 0. \tag{1d}$$

The state of the SO is defined by the variable $x \in \mathbb{R}^n$, and the control inputs are defined by $u \in \mathbb{R}^m$. The boundary conditions are described by the function $g(x_0,t_0,x_f,t_f)$, and the dynamics of the SO are given by $f(x,u,t)$. Furthermore, the performance index $V(x_{s,f},t_f,\theta)$ and the Lagrangian $\mathscr{L}(x,u,p,t)$ describe the terminal and stage cost, respectively [8]. To obtain the minimum time version of the formal OCP, a cost function is derived using the Hamilton Jacobi Bellman partial differential equation (HJB PDE) [8]. Rearranging the Bolza form into differential form [9], then yields

$$\frac{\partial V}{\partial t} + \sup_{u\in U}[\mathscr{L}(x,u,p,t) + p^T f(x,u,t)] = 0. \tag{2}$$

The HJB PDE solution will provide us with a path to finding the minimum time reachability solution set as proven by Crandall et al [10]. As shown in [3][11], by removing the stage cost, i.e., Lagrangian ($\mathscr{L}(x,u,p,t) = 0$), only the terminal cost remains, which provides the necessary formulation for maximizing reachable distances in a given time-horizon.This yields the following form of the problem

$$\frac{\partial V}{\partial t} + \sup_{u\in U}[p^T f(x,u,t)] = 0. \tag{3}$$

2.2 Sampling Methods for Subspace Reachability

With the formulation of the problem as a simplified HJB PDE and the understanding that the solution of this PDE yields the minimum time reachable set, the reachability computation is performed on a subspace ($\mathbb{R}^s$) of the full state space ($\mathbb{R}^n$). This is accomplished by projecting the full reachable set onto a subspace of interest as seen in Fig. 1 below.

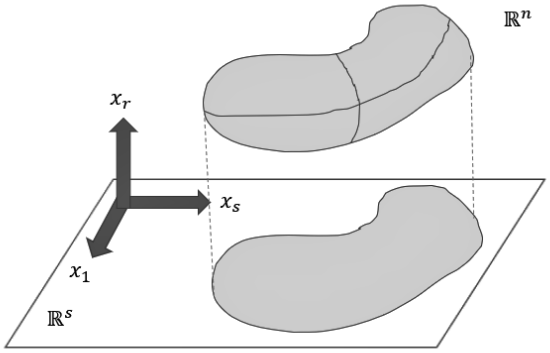

Fig. 1: Subspace reachability projection visualization.

To accomplish this, the performance index function, $V(x_{s,f}, t_f, \theta)$, is defined as

$$V(x_{s,f}, t_f, \theta) = \frac{1}{2} x_{s,f}^T | R(\theta) D R(\theta)^T x_{s,f} = \frac{1}{2} x_{s,f}^T G x_{s,f}, \tag{4}$$

where G represents a search direction in the position subspace, obtained via the rotation matrix $R(\theta) \in \mathbb{R}^{sxs}$ and direction vector $D = \hat{e}_1 \hat{e}_1^T$ [4]. Substituting this index function into the simplified HJB PDE derived above in Eq. 4 yields the following result

$$\sup_{u \in U} \frac{1}{2} x_f^T \begin{bmatrix} G_{sxs} & 0_{sxr} \\ 0_{rxs} & 0_{rxr} \end{bmatrix} x_f, \tag{5a}$$

$$\dot{x} = f(x, u, t), \tag{5b}$$

$$g(x_0, t_0) = 0, \tag{5c}$$

where the final state is denoted by x_f, the matrix G captures the position space of interest, and the solution of this optimal control problem yields the position reachable set. Before this can be solved in a computationally efficient manner, the initial states under consideration must also be defined. To do this, the initial state is constrained by the initial manifold $g(x_0, t_0)$, which is the surface of an ellipsoidal set, motivated by the frequent use of Gaussian probability distributions as descriptors of state uncertainty [12]. This initial state thus satisfies

$$g(x_0, t_0) = 0 = x_0^T E x_0 - 1. \tag{6}$$

Using this set of possible initial conditions, numerical continuation methods are then applied to solve the position reachability problem by finding solutions that satisfy the boundary conditions. This requires finding the roots of the vector function [3]

$$F[z(s), s] = 0, \tag{7}$$

where $s \in \mathbb{R}$ is the scalar continuation parameter and

$$F = \begin{bmatrix} \frac{\partial V}{\partial x_f}^T (x_f) - p_f \\ g(x_0) \end{bmatrix} \tag{8}$$

$$z = \begin{bmatrix} x_0 \\ \lambda \end{bmatrix} \tag{9}$$

As the continuation parameter changes, the solution to the corresponding optimal control problem z will also change. Due to dependence on the continuation parameter and the root finding nature of the problem, the derivative with respect

to s must be zero, that is,

$$\frac{dF[z(s),s]}{ds} = 0. \tag{10}$$

Applying the chain rule to (10) yields

$$\frac{dF}{ds} = \frac{\partial F}{\partial z}\frac{dz}{ds} + \frac{\partial F}{\partial s} = 0, \tag{11}$$

and re-arranging (11) yields the following initial-value problem in terms of the continuation parameter

$$\frac{dz}{ds} = -\left[\frac{\partial F}{\partial z}\right]^{-1}\frac{\partial F}{\partial s}. \tag{12}$$

The initial-value problem can be solved using a variety of numerical integration techniques as long as the Jacobian, $\frac{\partial F}{\partial z}$, remains invertible throughout.

2.3 The Minimum Enclosing Ball

The minimum enclosing ball computation is necessary as the result leads to an efficient focal plane projection that ultimately leads to a conservative custody determination probability. The conservatism of this custody determination is due to the fact that the minimum enclosing ball is guaranteed to be an over-approximation of the true subspace reachable set. The algorithm for computing the minimum enclosing ball used in this paper is Welzl's algorithm [13] and has computational complexity $O(n)$. This method of surface determination was chosen over other methods for computing a surface for projection such as convex hull fitting as they have a $O(n\log n)$ lower bound on their computational complexity.

2.4 Reachability Based Custody Probability

The position reachable set is the one that uniquely determines how and when custody may be lost and as such is used to quantify a probability of custody. Furthermore, no assumptions are made about the observer other than that it is optical in nature with a specific field of view (FOV) θ. Given the x-y-z position of an observer r_{obs} and space object r_{so}, the estimated range vector from the observer to the space object is $\rho = r_{\text{so}} - r_{\text{obs}}$.

The ultimate goal of this analysis is to determine an area for the field of view that the area of the reachable set can be projected on to. As such, an area-based probability measure is constructed that represents a degree of custody. This probability measure follows the definition of custody presented in [14] where if the position reachable set is contained inside telescope FOV, then custody is guaranteed over that specific time horizon. Recognizing that the maximum distance an observer can view along the sensor plane is

$$d_{\text{fov}} = ||\rho||sin(\theta), \tag{13}$$

the square area of the observer FOV is calculated, denoted A_{fov}. As previously mentioned the position reachable set is over-approximated using the minimum enclosing ball that, in two dimensions, has an area of $A_r = \pi r_{\text{ball}}^2$, where r_{ball} is the radius of the sphere. Using these areas, the probability of custody is defined as

$$p_{\text{c}} = \begin{cases} 1 & A_r < A_{\text{fov}}, \\ \frac{A_r - A_{\text{fov}}}{A_r} & A_r > A_{\text{fov}}. \end{cases} \tag{14}$$

3. CUSTODY LOSS TIME HORIZON DETERMINATION

Using the above presented theory it is now possible to describe the process for the determination of a time horizon where custody will be lost. This time horizon also corresponds to the amount of time that an observer can stop observing a SO before needing to re-observe. This approach is agnostic to the location of the observer as long as the sensor has a known field of view.

The general process uses sampling-based reachable sets to approximate the position reachable set. Then, the minimum enclosing ball is calculated and projected onto the sensor field of view to determine a probability of custody. This algorithm takes in a user-defined probability of custody and then iterates through time horizons to determine when custody is lost according to the provided specification.

Algorithm 1 Custody Loss Time Horizon Determination

Require: $p_c, \theta, r_{so}, r_{obs}$
$A_{fov} = ||r_{so} - r_{obs}||sin(\theta)$ ▷ From the FOV determine the A_{fov}
$A_{r-cl} = \frac{1-p_c}{A_{fov}}$ ▷ Determine the area of the reachable set enclosing ball needed for custody loss.
$A_r = 0$ ▷ Initialize the current area of the enclosing ball.
$t = 0$ ▷ Initialize time horizon in days.
while $A_r \leq A_{r-cl}$ **do** ▷ Iterate through the reachable set computations incrementing the time horizon.
$A_r \leftarrow computeReach(t)$
$t \leftarrow t + 1$
end while

3.1 The Circular Restricted Three Body Problem

The circular restricted three body problem is commonly used as an approximation for the dynamics in the Earth-Moon three body system. In this approximation, two spherical celestial bodies are restricted to Keplarian motion while a third, infinitesimal mass, moves under the influence of the two bodies. Due to the infinitesimally small mass of the third body, it is assumed that the two celestial bodies affect the motion of the third but are not, in turn, affected by it. Another key assumption to the circular restricted three body problem is that the two celestial bodies are in circular orbits around a combined center of mass known as the system barycenter. Fig. 1 below depicts the restricted three body problem with a rotating frame $\mathscr{F} : [\mathscr{B}, \hat{x}, \hat{y}, \hat{z}]$ whose origin is located at the barycenter $\mathscr{B}$. This paper will focus on the case where m_1 represents the Earth, m_2 represents the Moon, and m_3 is a space object of interest. These three bodies will rotate about the system barycenter at a known angular rate of ω and are separated by distances ρ_1, ρ_2, and r.

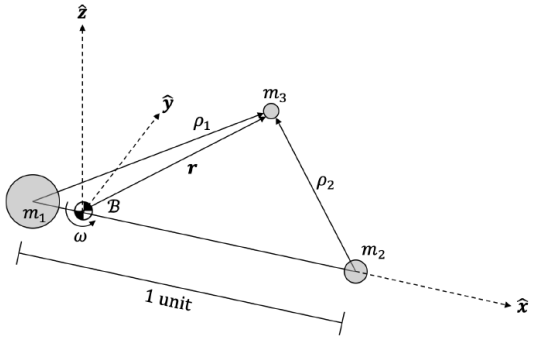

Fig. 2: Circular Restricted Three Body Problem Diagram [15]

The dynamics of a state $X = [x, y, z, \dot{x}, \dot{y}, \dot{z}]$ defined with respect to the rotating frame described above that follow the circular restricted three body assumptions are given by [16]

$$\ddot{x} = 2\dot{y} + x - (1-\mu)\frac{x-x_1}{\rho_1^3} - \mu\frac{x-x_2}{\rho_2^3} + \bar{u}_x \tag{15a}$$

$$\ddot{y} = -2\dot{x} + (1 - \frac{1-\mu}{\rho_1^3} - \frac{\mu}{\rho_2^3})y + \bar{u}_y \tag{15b}$$

$$\ddot{z} = (-\frac{1-\mu}{\rho_1^3} - \frac{\mu}{\rho_2^3})z + \bar{u}_z \tag{15c}$$

These dynamics are defined to be the time derivatives with respect to the non-dimensional time $\tau = \omega t$. Furthermore, (x, y, z) are normalized using the distance and mass ratios seen in Equations (16b)-(16c) below. The control inputs

$(\bar{u}_x, \bar{u}_y, \bar{u}_z)$ are non-dimensional and normalized similarly.

$$\rho_1 = \sqrt{(x+\mu)^2 + y^2 + z^2} \tag{16a}$$

$$\rho_2 = \sqrt{((x+\mu-1)^2 + y^2 + z^2} \tag{16b}$$

$$\mu = \frac{m_2}{m_1 + m_2} \tag{16c}$$

Using these dynamics and appropriate initial conditions, the motion of a SO in cislunar space can be used in the above reachability analysis to determine the position reachable set after a desired time horizon.

4. RESULTS AND DISCUSSION

Initially the above method is applied to a space object placed near the L1, L2, L3, L4, and L5 Lagrange points. From here, the method is applied to a space object placed in the Gateway orbit to provide a concrete example of the methods ability to apply to a well known real world scenario.

These simulations focus on a spacecraft modeled after the Lunar IceCube 6U CubeSat that has a maximum thrust of 0.8 mN and mass of 14 kg [17]. This spacecraft was chosen as it represents a real world mission in cislunar space. Furthermore, it was assumed that this thrust could be exerted independently in a three-thruster configuration where each is aligned with an axis in the rotating frame $\mathscr{F} : [\mathscr{B}, \hat{x}, \hat{y}, \hat{z}]$ described above.

4.1 Lagrange Point Results

The following figures (Fig. 3a - Fig. 12b) depict the results of the Lunar IceCube 6U CubeSat being placed near each of the Lagrange points. These figures are first presented at scale using the Moon, L1, and L2 for reference and then in subsequent plots the reachable sets are zoomed in on. The process of zooming in on the position reachable set acts to provide a better understanding of how the reachable set evolves over different time horizons. Furthermore, the dashed circles represent the minimum enclosing ball that was calculated as described in Section 2.3. Each of the Lagrange point simulations were propagated for a time horizon of one and five days. A key trend to recognize is that as the time horizon is increased from one to five days the reachable set extends asymmetrically, which is caused by the unstable dynamics in the cislunar region. Furthermore, as the time horizon increases the minimum enclosing ball will produce an increasingly larger over-approximation on the position reachable set. Ultimately, this will provide a conservative estimation of the probability of custody loss as the time horizon is increased according to the algorithm presented in Section 3. After directly calculating the area of the minimum enclosing ball the presented algorithm could be applied to an observer with a known field of view in addition to a desired probability of custody maintenance.

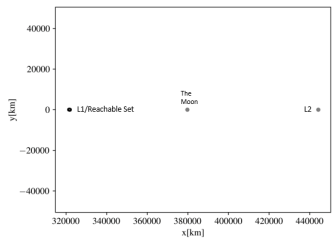

(a) Projection of the position reachable set over-approximation on the X-Y plane propagated for 1 day near L1.

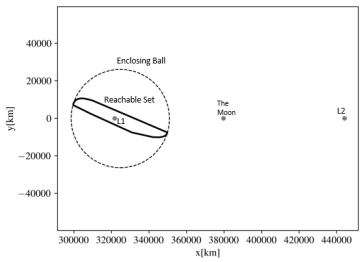

(b) Projection of the position reachable set over-approximation on the X-Y plane propagated for 5 days near L1.

Fig. 3: Figures depicting the reachable set near L1 after 1 and 5 days with the Moon and L2 as a reference for scale.

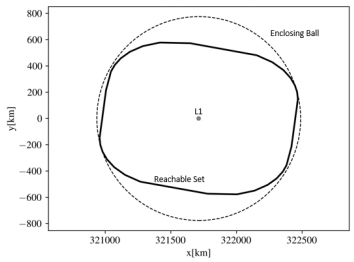

(a) Projection of the position reachable set over-approximation on the X-Y plane propagated for 1 day near L1.

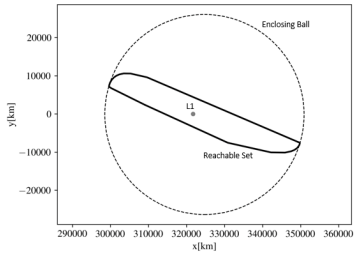

(b) Projection of the position reachable set over-approximation on the X-Y plane propagated for 5 days near L1.

Fig. 4: Figures depicting the reachable set near L1 after 1 and 5 days.

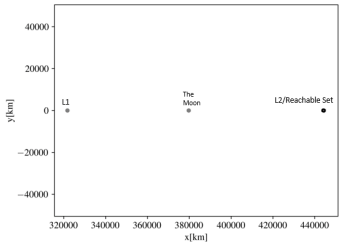

(a) Projection of the position reachable set over-approximation on the X-Y plane propagated for 1 day near L2.

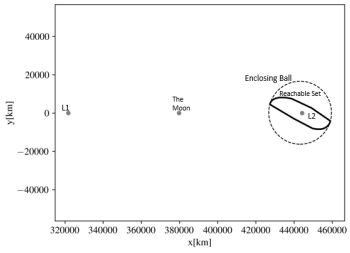

(b) Projection of the position reachable set over-approximation on the X-Y plane propagated for 5 days near L2.

Fig. 5: Figures depicting the reachable set near L2 after 1 and 5 days with the Moon and L1 as a reference for scale.

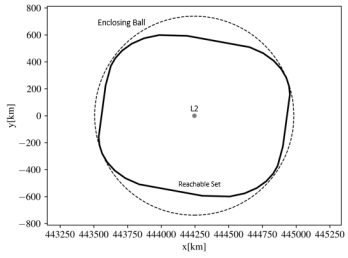

(a) Projection of the position reachable set over-approximation on the X-Y plane propagated for 1 day near L2.

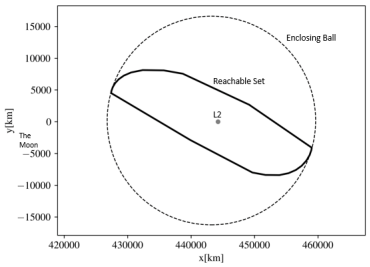

(b) Projection of the position reachable set over-approximation on the X-Y plane propagated for 5 days near L2.

Fig. 6: Figures depicting the reachable set near L2 after 1 and 5 days.

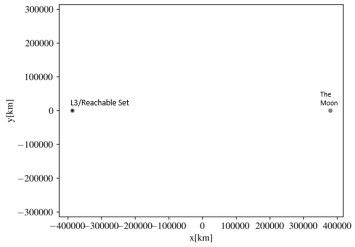

(a) Projection of the position reachable set over-approximation on the X-Y plane propagated for 1 day near L3.

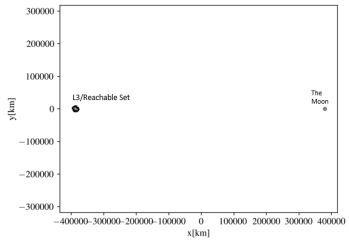

(b) Projection of the position reachable set over-approximation on the X-Y plane propagated for 5 days near L3.

Fig. 7: Figures depicting the reachable set near L3 after 1 and 5 days with the Moon as a reference for scale.

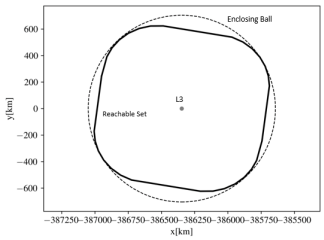

(a) Projection of the position reachable set over-approximation on the X-Y plane propagated for 1 day near L3.

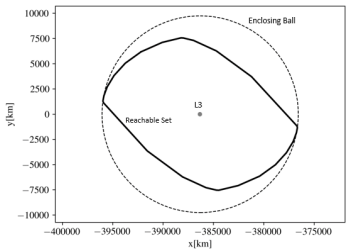

(b) Projection of the position reachable set over-approximation on the X-Y plane propagated for 5 days near L3.

Fig. 8: Figures depicting the reachable set near L3 after 1 and 5 days.

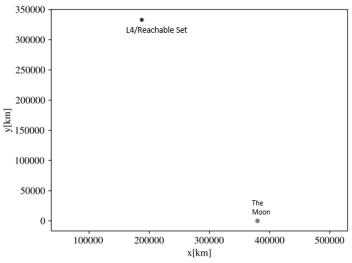

(a) Projection of the position reachable set over-approximation on the X-Y plane propagated for 1 day near L4.

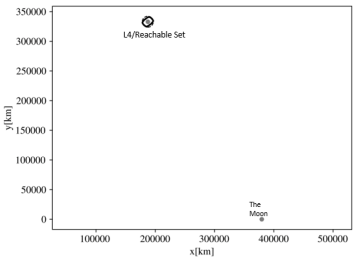

(b) Projection of the position reachable set over-approximation on the X-Y plane propagated for 5 days near L4.

Fig. 9: Figures depicting the reachable set near L4 after 1 and 5 days with the Moon as a reference for scale.

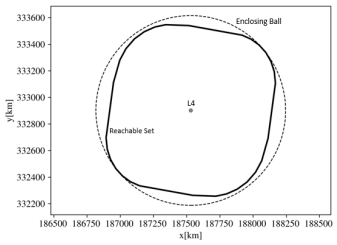

(a) Projection of the position reachable set over-approximation on the X-Y plane propagated for 1 day near L4.

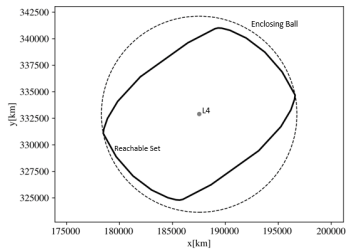

(b) Projection of the position reachable set over-approximation on the X-Y plane propagated for 5 days near L4.

Fig. 10: Figures depicting the reachable set near L4 after 1 and 5 days.

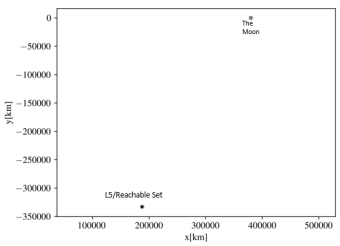

(a) Projection of the position reachable set over-approximation on the X-Y plane propagated for 1 day near L5.

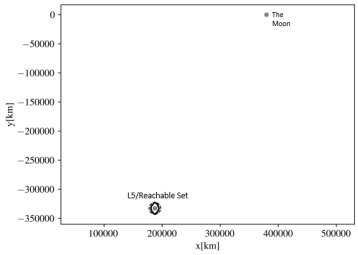

(b) Projection of the position reachable set over-approximation on the X-Y plane propagated for 5 days near L5.

Fig. 11: Figures depicting the reachable set near L5 after 1 and 5 days with the Moon as a reference for scale.

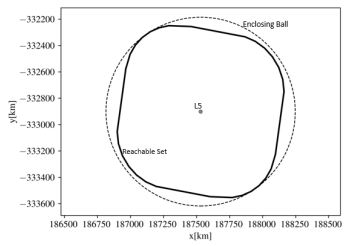

(a) Projection of the position reachable set over-approximation on the X-Y plane propagated for 1 day near L5.

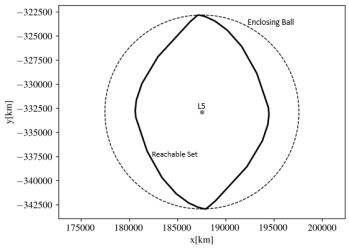

(b) Projection of the position reachable set over-approximation on the X-Y plane propagated for 5 days near L5.

Fig. 12: Figures depicting the reachable set near L5 after 1 and 5 days.

4.2 Gateway Orbit Results

The following figures (Fig. 13a - Fig. 15c) depict the results of the Lunar IceCube 6U CubeSat being placed near apolune on the Lunar Gateway orbit. These figures are presented in order of the time horizon evolution from one to three days. For each time horizon a set of figures depicting the reachable set in the context of the orbit, the position reachable sets, and the minimum enclosing ball can be seen below. As with the two dimensional cases presented above, the minimum enclosing ball acts as an increasing over approximation for the position reachable set as the time horizon is increased. Furthermore, in the case of this orbit, the position reachable set computation was performed up to the three day time horizon because it becomes numerically unstable as perilune is approached. This is because perilune is where the smallest perturbations in the dynamics will yield the largest changes. The minimum enclosing ball approximation can be projected onto each axis for ease of area determination. From here the algorithm could be applied to any observer with a known field of view in addition to a desired probability of custody.

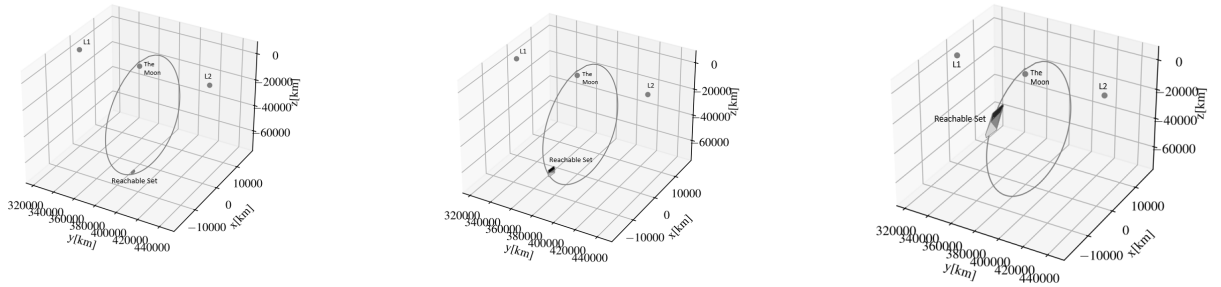

(a) Projection of the position reachable set over-approximation on the X-Y-Z plane propagated for 1 day on the Gateway orbit near apolune.

(b) Projection of the position reachable set over-approximation on the X-Y-Z plane propagated for 2 days on the Gateway orbit near apolune.

(c) Projection of the position reachable set over-approximation on the X-Y-Z plane propagated for 3 days on the Gateway orbit near apolune.

Fig. 13: Figures displaying the orbits and reachable set for each time horizon.

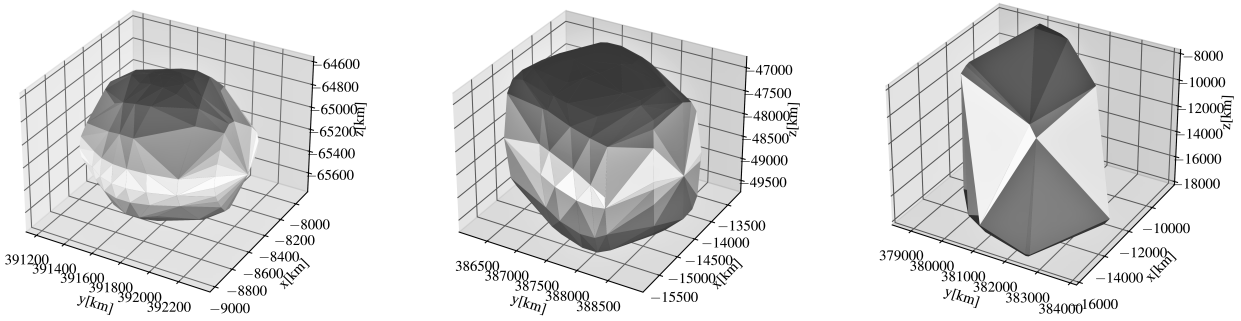

(a) Zoom in on the position reachable set projection after 1 day.

(b) Zoom in on the position reachable set projection after 2 days.

(c) Zoom in on the position reachable set projection after 3 days.

Fig. 14: Figures displaying the position reachable set for each time horizon.

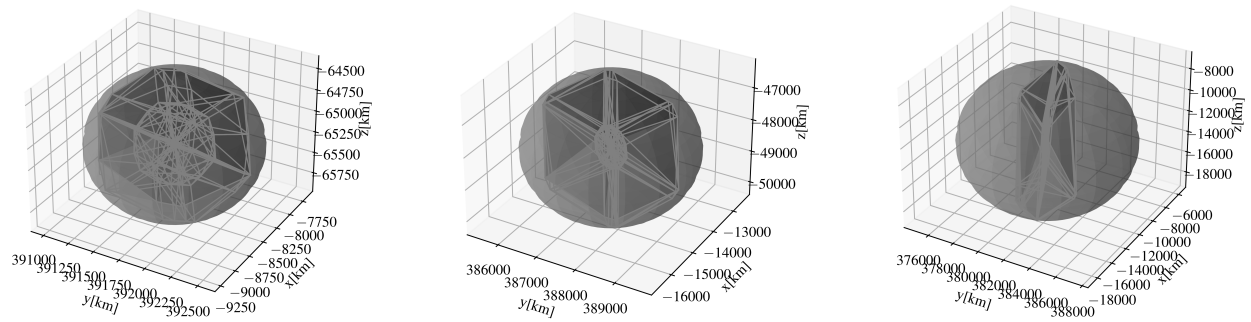

(a) Minimum enclosing ball for the position reachable set projection after 1 day.

(b) Minimum enclosing ball for the position reachable set projection after 2 days.

(c) Minimum enclosing ball for the position reachable set projection after 3 days.

Fig. 15: Figures displaying the minimum enclosing ball for each time horizon.

5. CONCLUSION

There is a wealth of possible resources that cislunar space could provide including in-situ construction of spacecraft or waypoints for interplanetary exploration as shown in [18]. An increasingly crowded cislunar environment will make create more challenges in telescope tasking. To address these challenges, reachability analysis was used to obtain a set of possible locations that an SO could end in given an initial set and some specified problem dynamics. Combining the reachability analysis with a metric for probability of custody combines into a novel method to obtain the time horizon after which custody will be lost. This method was applied to the L1, L2, L3, L4, L5 Lagrange points and the Lunar Gateway orbit. This was done to provide results depicting the evolution of reachable sets with time horizon that can then be applied to any observer with a known FOV to perform custody determination and complete the loop presented in Section 3.

6. REFERENCES

[1] JOHN W RAYMOND. Space capstone publication, spacepower (scp) headquarters united states space force june 2020 dedicated to past, present, and future spacepower pioneers. 2020.

[2] MJ Holzinger, CC Chow, and P Garretson. A primer on cislunar space.

[3] Marcus J Holzinger and Daniel J Scheeres. Reachability results for nonlinear systems with ellipsoidal initial sets. *IEEE transactions on aerospace and electronic systems*, 48(2):1583–1600, 2012.

[4] Marcus J Holzinger and Daniel J Scheeres. Reachability set subspace computation for nonlinear systems using sampling methods. In *2011 50th IEEE Conference on Decision and Control and European Control Conference*, pages 7317–7324. IEEE, 2011.

[5] Inseok Hwang, Dušan M Stipanovic, and Claire J Tomlin. Applications of polytopic approximations of reachable sets to linear dynamic games and a class of nonlinear systems. In *Proceedings of the 2003 American Control Conference, 2003.*, volume 6, pages 4613–4619. IEEE, 2003.

[6] Alexander B Kurzhanski and Pravin Varaiya. Ellipsoidal techniques for reachability analysis. In *International Workshop on Hybrid Systems: Computation and Control*, pages 202–214. Springer, 2000.

[7] Daniel Aguilar Marsillach, Shahzad Virani, Marcus J Holzinger, Moses W Chan, and Prakash P Shenoy. Real-time telescope tasking for custody and anomaly resolution using judicial evidential reasoning. In *29th Space Flight Mechanics Meeting, AAS Paper*, pages 19–534, 2019.

[8] PD Loewen and RT Rockafellar. Bolza problems with general time constraints. *SIAM journal on control and optimization*, 35(6):2050–2069, 1997.

[9] John Lygeros. On the relation of reachability to minimum cost optimal control. In *Proceedings of the 41st IEEE Conference on Decision and Control, 2002.*, volume 2, pages 1910–1915. IEEE, 2002.

[10] Michael G Crandall, Lawrence C Evans, and P-L Lions. Some properties of viscosity solutions of hamilton-jacobi equations. *Transactions of the American Mathematical Society*, 282(2):487–502, 1984.

[11] Julian Brew, Marcus J Holzinger, and Stefan R Schuet. Reachability subspace exploration using continuation methods. In *AAS/AIAA Space Flight Mechanics Meeting*, 2017.
[12] Arthur Gelb. *Applied optimal estimation*. MIT press, 1974.
[13] Emo Welzl. Smallest enclosing disks (balls and ellipsoids). In *New results and new trends in computer science*, pages 359–370. Springer, 1991.
[14] Daniel Aguilar Marsillach and Marcus J Holzinger. Telescope tasking for maneuver detection and custody maintenance using evidential reasoning and reachability theory. 2020.
[15] Jacob K Vendl and Marcus J Holzinger. Cislunar periodic orbit analysis for persistent space object detection capability. *Journal of Spacecraft and Rockets*, pages 1–12, 2021.
[16] Hanspeter Schaub and John L Junkins. *Analytical mechanics of space systems*. Aiaa, 2003.
[17] Natasha Bosanac, Andrew D Cox, Kathleen C Howell, and David C Folta. Trajectory design for a cislunar cubesat leveraging dynamical systems techniques: The lunar icecube mission. *Acta Astronautica*, 144:283–296, 2018.
[18] Carlos Manuel Entrena Utrilla. Establishing a framework for studying the emerging cislunar economy. *Acta Astronautica*, 141:209–218, 2017.